2014-12

Surface Enhanced Raman Scattering with gold nanoparticles: Effect of particle shape

Furong Tian
Technological University Dublin, furong.tian@tudublin.ie

Franck Bonnier
Technological University Dublin, Franck.Bonnier@tudublin.ie

Alan Casey
Technological University Dublin, alan.casey@tudublin.ie

See next page for additional authors

Recommended Citation

Tian, F. et al. (2014)Surface Enhanced Raman Scattering with gold nanoparticles: Effect of particle shape, *Analytical Methods,* 6, pp.9116-9123. doi:10.1039/C4AY02112F

Funder: EU Marie Curie IF

Analytical Methods

RSCPublishing

Paper

Surface Enhanced Raman Scattering with gold nanoparticles: Effect of particle shape

Cite this: DOI: 10.1039/x0xx00000x

Furong Tian*, Franck Bonnier, Alan Casey, Anne E. Shanahan, Hugh J. Byrne

Received 00th January xxxx,
Accepted 00th January xxxx

DOI: 10.1039/x0xx00000x

www.rsc.org/methods

The dependence of the Surface Enhanced Raman Scattering (SERS) by gold nanoparticles on their shape is examined using the organic dye, rhodamine 6G (R6G) as probe molecule. SERS has been explored extensively for applications in sensing and imaging, but the design and optimisation of efficient substrates is still challenging. In order to understand and optimise the SERS process in nanoparticles, gold nanospheres and their aggregates, nanotriangles, and nanostars of similar dimensions were synthesised and characterised according to their average size, zeta potential and UV/visible absorption. SERS from R6G was negligible for unaggregated nanospheres at 532 nm, close to the maximum of the surface plasmon resonance (SPR) at 560 nm. Upon aggregation of the nanospheres, the SPR shifts to ~660 nm, attributable to local surface plasmon "hotspots" between the spheres, and the SERS signal of R6G is significantly increased, at 785 nm. In monodisperse gold nanotriangles, the SPR is located at ~800 nm, and significant SERS of R6G is observed using 785 nm as source, as is the case for gold nanostars, which exhibit a double SPR with maxima at ~600 nm and ~785 nm, attributable to the core sphere and vertices of the structures, respectively. In suspensions of equal nanoparticle and dye concentration, the SERS effect increases as nanospheres<nanosphere aggregates <nanotriangles<nanostars, clearly indicating that control over the number of local field hotspots can optimise the SERS efficiency. Notably, it is demonstrated that the SERS intensity per nanoparticle scales with the magnitude of the SPR absorbance at the excitation wavelength (785 nm), providing a clear guide to optimisation of the process experimentally.

1. Introduction

Gold nanoparticles (GNPs) are biocompatible and have advantageous optical properties for biomedical applications [1]. GNPs with different geometry, such as spheres, rods, triangles, hexagons, prisms, urchins, cubes, wires and stars have been explored for specific biomedical applications in dispersed form [2]. In this context, surface-enhanced Raman scattering/spectroscopy (SERS) has attracted a great deal of attention as a sensitive technique for chemical and bioanalytical sensing and imaging [2, 3]. There exists a plethera of work which has been performed to demonstrate SERS effects for different molecules, with different shaped nanoparticles, at different dosages [4], so much so that it is not easy to establish the principle parameters which need to be optimised for effective and reproducible SERS. The development of reliable quantitative comparisons is a priority which is required for meaningful design strategies for new nanomaterials. The purpose of this study is to identify critical conditions and physical properties of the materials which play the main role in optimised SERS.

Address, FOCAS Research Institute, Dublin Institute of Technology, Kevin Street, Dublin 8, Ireland. Fax: + 00 353 1 402 7901; Phone: 00 353 (0)1 402 7982; E-mail: fuormg.tian@dit.ie

Although the SERS effect in metal nanoparticles is proposed to derive from the local fields associated with the excitation of surface plasmon resonances by the Raman source, nanospheres suffer from low enhancement levels that vary widely from particle-to-particle and fluctuate with their environment [5]. In fact, more recent explanations of SERS on metal nanoparticles are based not on intrinsic nanoparticle surface plasmons, but local field "hotspots" [6] due to surface roughness [7], between aggregated metallic NPs [8] or between nanoparticles [9] and a metal surface [10] and that the SERS contribution of such hotspots can dominate the observed response [11]. An alternative way to increase the local electromagnetic field associated with SPR is to increase, in a systematic fashion, the local curvature of nanomaterials. A 10-100 times higher field strength was estimated at the vertices of silver nanotriangles compared to the surface of nanospheres [12]. Recently, a new class of star-shaped gold nanoparticle with sharp edges and tips, referred to as nanostars, has been shown to exhibit a very high sensitivity to local changes in the dielectric environment, as well as larger enhancements of the electric field around the nanoparticles [13]. Similar results have been found for other nanoparticles with sharp features [4, 14].

The methods to produce gold nanospheres, nanotriangles and nanostars with a high degree of control of the size/shape distribution can be considered as routine, and thus a direct comparison of the SERS efficiency of the different structures is warranted. This study will detail the synthesis and UV/visible absorption of such nanoparticles, and will explore their relative efficiencies for SERS

using the organic dye molecule rhodamine 6G (R6G) as a probe, in an attempt to elucidate routes towards optimised SERS probes. Aggregation of nanospheres is induced to demonstrate the further enhancement due to interparticle local field "hotspots" and to compare with the intrinsic enhancement induced at the vertices of nanotriangles and nanostars.

2. Experimental

$HAuCl_4H_2O$, $NaBH_4$, ascorbic acid, $AgNO_3$, cetyl-trimethylammonium bromide (CTAB), and 10nm gold colloid suspensions (6 x 10^{12} /mL) were purchased from Sigma Aldrich (Dublin, Ireland). Ultrapure deionized water (resistivity greater than 18.0 $M\Omega cm^{-1}$) was used for all solution preparations and experiments [15].

Gold nanospheres, with diameter ~150 nm, were prepared using the seed-mediated growth method [15]. 0.01 mL of the 10 nm gold colloid seed suspension (Sigma Aldrich) was added to 10 mL of the reducing solution, containing trisodium citrate and ascorbic acid, under vigorous stirring over a time of ~45 min. Immediately after the addition was complete, the mixture was brought to the boil and maintained at this temperature for ~30 min. In order to evaluate the effect of aggregation on SERS from the gold nanospheres, acidic conditions were employed to induce nanoparticle aggregation [16]. HCl at a concentration of 1 M was added dropwise to aqueous suspensions of 150 nm nanospheres and the pH value was adjusted between 7 to 4. At pH=4, the particle solution was seen to undergo a colour change indicative of aggregation[17].

Gold nanotriangles were prepared by a reduction of chloroauric acid ($HAuCl_4$) using sodium thiosulfate as reducing agent [1, 18]. The synthesis requires aqueous ascorbic acid (75 mL, 10 mM), and 0.01 mL of the 10 nm gold colloid suspension (Sigma Aldrich) in 5 mL distilled water, to which 3 mL of 0.5 mM $AgNO_3$ is added at a rate of 1 mL/min. 150 μL of 10 mM ascorbic acid solution and 0.5 mM $HAuCl_4$ are then added at 0.2 mL/min while stirring vigorously. Within the initial 5 min of the reaction, the colour of the solution changed from yellow (gold salt) to brownish. This change of colour indicated the formation of GNPs. The reaction was stopped after 15 minutes, to limit the particle size to ~120nm and prevent aggregation, by centrifugation of the nanoparticles [19]. Nanotriangles were subsequently washed by deionized water three times under centrifugation at 4500 RPM for 15 mins.

Gold nanostars were prepared in aqueous phase via the surfactant-directed, seed-mediated growth method as described in the literature [20]. Growth solution was prepared by adding 0.20 mL of 0.01 M $HAuCl_4$:4H2O to 4.5 ml of 0.1 M CTAB in a plastic test tube while gently mixing. To this solution, 0.030 mL of 0.01 M $AgNO_3$ was added. After mixing, the colour of the solution becomes brownish yellow. Then, 0.032 mL of 0.1 M ascorbic acid was added, resulting in a colourless solution. Finally, 0.01 mL of the 10 nm gold colloid suspension (Sigma Aldrich) was added. After gentle mixing, the solution was kept in a water bath at room temperature. The eventual blue-purple colour of the growth solution indicates gold nanostar formation [20]. The reaction was stopped after 30 minutes, to limit the particle size to ~150nm and prevent aggregation [21]. Khoury et al. have demonstrated that prolonged reaction time can result in increased size of nanostars [21]. Nanostars were subsequently washed by deionized water three times under centrifugation at 4500 RPM for 15 mins. The surfactant CTAB and ascorbic acid were removed by washing with water. Once the reaction was stopped and the products remained stable over 6 months.

A Perkin Elmer Lambda 900 UV/VIS/NIR Spectrometer and Zetasizer Nano ZS analyser (Malvern Instruments, Worcestershire, UK) were used to measure the absorbance, hydrodynamic particle size and zeta potentials of the nanoparticles and to observe the formation and/or aggregation of NPs.

In parallel, the three different geometry nanoparticles (spheres, triangles, star) as well as nanosphere aggregates, at a nanoparticle number concentration (Nn) of 3 x 10^3 particle/mL, were deposited on a 300-mesh grid for TEM (Ted Pella Formvar/Carbon type B) by drop casting 10 μL of the aqueous solution of nanoparticles. Similar nanoparticle solutions were dropped onto prewashed silicon substrates and spin coated at a speed of 1000 rpm for 20 seconds for SEM. The samples were dried in air and characterised by Electron Microscopy using a Hitachi SU6600 FESEM instrument at an acceleration voltage of 25 kV. Scanning EM images were taken using the SE detector and the Scanning Transmission EM images were taken using the TE detector.

Raman spectroscopy was performed with a HORIBA Jobin Yvon HR800 spectrometer with either a 50 mW 532 nm or a 300 mW 785 nm diode laser as source. Spectral data was collected using a 10× microscope objective over the range 400–1800 cm^{-1} with a 10 sec integration time. The detector used was a 16-bit dynamic range Peltier cooled CCD detector [22, 23].

SERS samples were prepared by mixing 25 μl of GNP solution with 25 μl of aqueous solutions of the probe molecule (R6G) at varying concentrations. In all cases, the nanoparticle number was estimated based on the concentrations of initial seed nanospheres. In the case of the aggregated nanospheres, nanoparticle numbers quoted for all experiments are those of the initial, unaggregated suspensions. Final nanoparticle concentrations (Nn) of 3 x 10^3, 3 x 10^6 or 3 x 10^9/mL were employed for the range of experiments. For the probe molecule, concentrations were varied over the ranges 0.1 – 10 μM (R6G), for each nanoparticle concentration. SERS effects in R6G have been well studied and, for example, it has been shown that silver can cause SERS on R6G in the μM range[24]. Solutions were dropped onto $CaFl_2$ substrates and measured immediately. For comparison, spectra of the probe molecule R6G alone were recorded from 1M aqueous solutions.

3. Results

3.1 Particle Sizing and Zeta Potential

Table 1 presents the key physicochemical characteristics within each group of nanoparticles used in the present study, as determined by a combination of DLS, Zeta potential, electron microscopy and absorption spectroscopy. In suspension, the DLS of the Gold nanosphere solutions indicates a monomodal dispersion with a hydrodynamic diameter of 150±9 nm and a zeta potential of -16.5±0.4 mV. In acidic conditions, the particle size distribution dramatically increases to 1030±37 nm, while the zeta potential is changed to -7.8±0.2 mV (Table 1). The acid reduces the absolute value of the negative zeta potential although it remains negative even at pH=4. Zeta potential is varied most commonly by pH adjustment [21].

Gold nanotriangles and nanostars similarly show a monomodal suspension with hydrodynamic diameters of 135±13 nm and 148±11 nm respectively, although it should be noted that the DLS algorithm for diameter calculation assumes spherical particles. The measured zeta potentials were -21.6±1.9 mV and 29.6±3.6 mV respectively.

Although they have been washed rigorously, the positive zeta potential of the nanostars, in contrast to the negative values observed for both other nanoparticles, is most likely due to residual cationic CTAB which is known to form bilayer structures on the surface of metals, resulting in a positive zeta potential [20]. However, it has been demonstrated that the shape of nanoparticles plays the dominant role in determining surface enhancement. Cube-like CTAB-capped gold nanoparticles were shown to provide 4 times higher SERS from human immunoglobulin G than spherical CTAB-capped gold nanoparticles[25].

Table 1. Physico-chemical characteristics of each different GNP type

Samples	Hydrodynamic Diameter (nm)	Zeta Potential (mv)	Number of vertices	Surface area (nm^2) per NP	λ_{max} nm
Nanosphere	150±9	-16.5±0.4	-	70650	560
Nanosphere +HCl	1030±37	-7.8±0.2	-	10,158	660
Nanotriangle	135±13	-21.6±1.9	3	62353	800
Nanostar	148±11	29.6±3.6	6	24335	600/ 785

3.2 Electron Microscopy

Electron microscopy was employed to confirm that the change in the DLS profile of the nanospheres in acidic conditions was due to aggregation, and to visualise the nanotriangles and nanostars in their isolated form. Figure 1 shows electron microscopy images of 150 nm gold nanospheres, precipitated from neutral (Figure 1a) and pH 4 (figure 1b-e) aqueous solutions. In the aggregated form, although isolated spheres are still evident, the bulk of the nanospheres exist as dimers, trimers or higher order aggregates. This is consistent with the observed dramatic increase in hydrodynamic diameter and lower zeta potential (Table 1). HCl decreases the absolute value of the zeta potential, resulting in a decreased repulsion between the NPs and consequent aggregation [16].

As shown in Figure 2 (a-c), nanotriangles, precipitated from aqueous solution of neutral pH, are flat regular structures with three congruent edge lengths in the 100 nm to 120 nm range. Typically, each tip is ~ 60 degrees (Fig. 2 a-c).

Nanostars typically have a central core and 6 vertices in a 3 dimensional arrangement. The length of the vertices is averaged at 35 nm and the angle at the vertex is less than 30 degrees (Fig. 2, d-f). Based on idealised geometric structures, nanospheres had the largest surface area per particle, followed by nanotriangles, while the nanostars had the smallest estimated surface area (Table 1). If a perfect spherical geometry is assumed, a hydrodynamic diameter of 1030nm for nanosphere aggregates yields a surface area of $3.3x10^6$ nm^2. Rationing the volumes of the nanosphere aggregates and nanospheres gives an estimate of 325 nanospheres per aggregate, and therefore a surface area per nanoparticle of ~1 x 10^4 nm^2 per nanosphere in an aggregate, less than that of the unaggregated nanospheres.

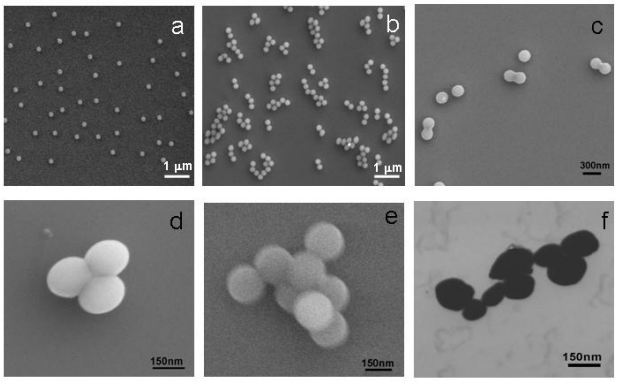

Figure 1: (a) SEM image of nanospheres, (b-e) SEM images of aggregated nanospheres: (f) shows an STEM image of aggregates of the same nanospheres.

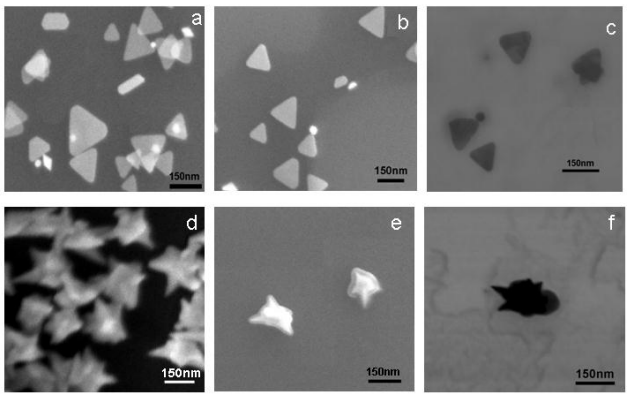

Figure 2: Electron microscopy images of nanotriangles (a-c) and nanostars (d-f). Images of (a), (b), (d) and (e) are taken by SEM. Images of (c) and (f) are STEM images.

3.3 UV-Vis-NIR absorption spectroscopy

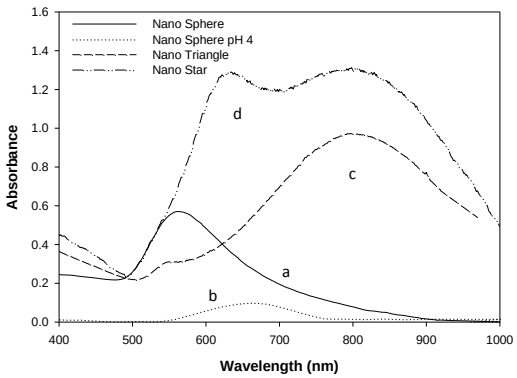

Figure 3: UV–vis absorption spectra of (a) nanospheres, (c) nanotriangles and (d) nanostars in aqueous solutions at a concentration of N_n of $6x10^8$ particles/ml. The dotted line in (b) illustrates the spectrum of the nanospheres in aqueous solution at pH 4.

Figure 3 shows the UV/vis/NIR absorption spectra of aqueous suspensions of the gold nanospheres, before (a - solid line) and after (b - dotted line) aggregation. Before aggregation, the spectral profile shows the SPR at λmax~560 nm, typical of gold nanospheres [26]. Upon the addition of HCl to the nanosphere solution, a colour change from red to blue-grey was immediately observable. The absorbance is dramatically reduced and the SPR band is red shifted to λmax ~ 660 nm. The observed behaviour is consistent with that previously reported for aggregation of gold nanospheres [26]. Notably, whereas the optimum wavelength for excitation of the SPR for monodisperse gold nanospheres is ~560 nm [27], that for aggregated nanospheres is substantially longer [26].

The spectrum of the nanotriangles shows a single SPR band at ~800 nm (Fig. 3c – dashed line). This feature corresponds to the in-plane dipolar mode, which falls in the near infrared range[28]. The positioning of the SPR maximum shifts to longer wavelength, from ~800 nm to ~950 nm, with reaction time, as a result of increasing particle size [19]. The nanostars show an absorbance spectrum which is doubly peaked, at ~600 nm and ~800 nm (Fig. 3d – dotted/dashed line). These two peaks derive from the two constituent structures of the nanostar, the spherical core and the peripheral vertices. The spherical core results in a SPR similar to the unaggregated nanospheres (Fig. 1a) while the multiple vertices contribute SPR in the near infrared range (Fig. 1d) [13]. The positioning of the second SPR peak increases from ~785 nm to ~900 nm, with reaction time, as a result of increasing particle size [21].

The optical properties of the GNPs in suspension thus reflect the characteristics of the local fields associated with the SPR. While the nanospheres have an intrinsic SPR at 560 nm, their aggregation, associated with the generation of local field hotspots between the spheres, causes a redshift of the SPR. In the case of the nanotriangles and the nanostars, the sharp vertices similarly act as local field hotspots resulting in SPRs shifted to the near infrared region of the spectrum [28, 29].

3.4 Raman Spectroscopy

As shown in Figure 4, Raman scattering was not observable under the measurement conditions employed in the presence of monodisperse gold nanospheres at a source wavelength of either 532 nm or 785 nm. At a pH=4, however, although no significant Raman scattering was observable using 532 nm as source, the Raman signal was significantly enhanced at 785 nm. Although 532 nm is close to the SPR band of the monodisperse nanospheres, no SERS effect is observed, consistent with the requirement for aggregation to generate local hotspots at which the local field is substantially enhanced, resulting in a shift of the SPR band to ~ 660 nm. In the aggregated suspensions, the particles are no longer resonant at 560 nm (Fig. 3a) and no SERS effect is observable using 532 nm as source, but a strong SERS signal is observable using 785 nm, as a result of the red shifted SPR.

In the absence of aggregation, the 785 nm laser is resonant with the primary SPR bands of both the nanostars and nanotriangles. These isotropic nanoparticles have strong SPR throughout the visible and near-IR (NIR) regions of the spectrum[29]. Figure 5a compares the Raman spectrum at 785nm of the 1M solution of R6G with the SERS spectrum of 5 μM R6G in a suspension of gold nanostars.

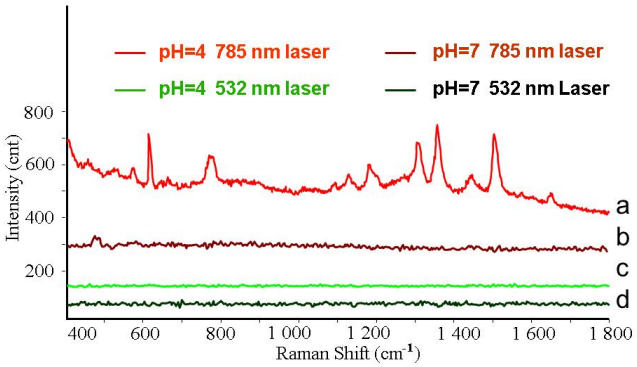

Figure 4: Raman spectra of gold nanosphere and 10 μM R6G using 532 nm and 785 nm as source. The red line shows molecules with nanospheres at 785 nm and pH=7 (a), the maroon line shows molecules with nanospheres at 785 nm and pH=4, the green line shows the spectra of molecules with nanospheres at 532 nm and pH=7 (c), the dark green shows the spectra of molecules with nanospheres at 532nm and pH=4 (d). The particle concentration is 3 x 10^9/ml. The spectra are offset for clarity.

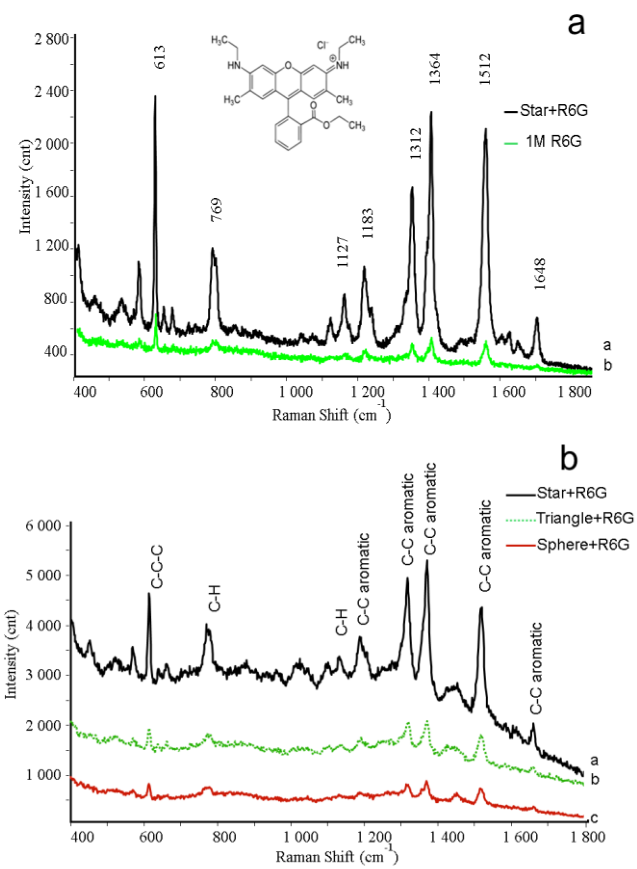

Figure 5: SERS spectra of R6G with aggregated-nanospheres, nanotriangles and stars at a concentration 3x10^9 particles/ml. (a) comparison of the SERS spectrum of 5 μM R6G in gold nanostar solution (a, dark), the Raman spectrum of 1 M R6G alone (b, green), (b) Comparison of 5 μM R6G SERS spectrum in solutions of gold nanostars (a, dark) nanotriangles (b, green dash) and aggregated nanospheres (c, red).

Three different groups of modes were observable for R6G, associated with C–C–C ring in-plane bending at 613 cm^{-1}, out-of-plane bending at 769 cm^{-1} and ring breathing (RB), such as aromatic C–C stretching at 1183, 1312, 1364, 1512 cm^{-1} and 1648 cm^{-1}, ν(C–H) at 1127 cm^{-1}. The vibrational modes observed in the SERS spectra (Fig. 5b) are assigned to the corresponding vibrational modes, consistent with the observations of SERS of R6G on silver nanospheres[30]. Consistent with literature [30, 31], eight Raman bands with strong scattering intensities are observed at 613, 775, 1130, 1278, 1364, 1389, 1512, and 1651 cm^{-1}. While all these modes were strongly enhanced on nanostars in the SERS measurements, only a few were detectable in the bulk Raman spectra of R6G. A comparison of SERS and Raman spectra of the molecule shows only small shifts of these modes, making it difficult to determine the adsorption site of the molecule on the GNP surface. The results suggest that R6G and GNPs do not interact strongly. On the other hand, the strong enhancements observed for all groups of modes mentioned previously suggests the central carbon atom, nitrogen atoms, and π electrons in the phenyl ring as possible interaction sites [24].

Significantly, in all measurements made, as shown in Figure 5b, the magnitude of the SERS response was highest for the gold nanostars, intermediate for the nanotriangles, lower for the aggregated nanospheres, and negligible for the unaggregated nanospheres (Fig. 3). The results are consistent with the requirement for enhanced electric fields at hotspots associated with aggregated nanospheres, or the vertices of triangular or star shaped nanoparticles.

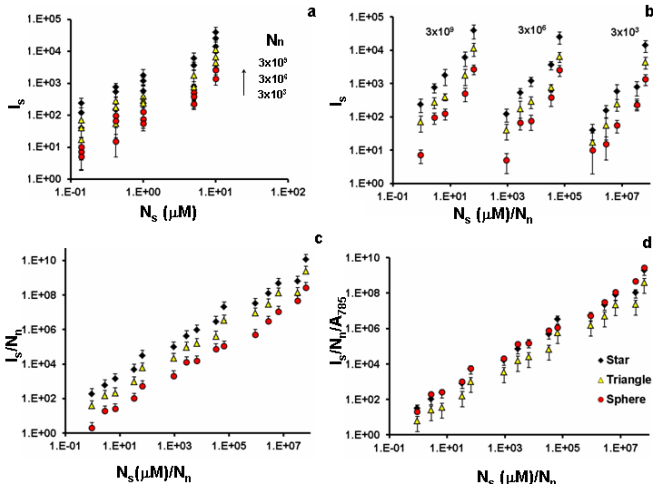

Figure 6: The intensity of the SERS peaks (above baseline) (I_S, arbitrary units) of R6G (1364cm^{-1}) at different concentrations of R6G (N_S, in μM) for each nanoparticle type (in each plot, Blue diamond=NanoStar, Yellow triangle = NanoTriangle, Red disc = aggregated Nanosphere) and each Nanoparticle number (N_n, per mL) range. (a) I_S vs N_S, (b) I_S vs N_S / N_n, (c) I_S /N_n vs N_S / N_n (d) I_S /N_n vs N_S / N_n normalised to absorbance at 785nm, A785.

Figure 6a plots the Raman intensity (I_S) of the 1364 cm^{-1} mode versus the dye concentration (N_S) for each nanoparticle concentration. For each nanoparticle type, there is a significant difference between the SERS intensity observed for a fixed nanoparticle concentration, and that signal is increased with the number of nanoparticles present at a given dye concentration. Note that the plot is log/log and the superlinear order of the slope for each curve (~ 1.2) indicates that the enhancement factor (normally defined as $EF = I_S N_R / I_R N_S$, where I_S and I_R are, respectively, the SERS and normal Raman intensities that result from sampling a concentration of N_S and N_R molecules [21]) is not independent of concentration of the dye or nanoparticles and the relationship between the Raman signal per dye molecule and the number of nanoparticles in solution is not immediately apparent.

The datasets are further separated when considering the Raman signal as a function of dye molecules per nanoparticle, as shown in Figure 6b. For each nanoparticle type, a similar SERS intensity is observed for substantially different regimes of the parameter I_s/ N_n, depending on the concentration of nanoparticles. However, when considering the SERS intensity per nanoparticle, as a function of the number of R6G molecules per nanoparticle, a more continuous behaviour is observed for each nanoparticle type, over the concentration range studied, as shown in Figure 6c.

In Figure 6c, a clear dependence of the SERS signal, and therefore enhancement factor, EF, on nanoparticle shape is observable. Although it is not accentuated in the log/log format of the graph, there remains a significant difference between the SERS per nanoparticle at a given concentration of dye per nanoparticle, in the sequence (aggregated) nanosphere < nanotriangle < nanostar.

3.5 Number of hotspots per particle

Given that the unaggregated nanospheres gave negligible SERS signals under these experimental conditions, the results clearly indicate that the number of intrinsic "hotspots" per particle (and for equal Nn, per unit volume) is a primary determinant on the SERS signal observable. This increases as nanospheres <nanotriangles <nanostars. Although it cannot be assumed that all "hotspots" are of equal strength, also implicit in the results is that the average number of hotspots per nanoparticle in aggregated nanospheres is significantly less than that in either nanotriangles or nanostars. This is also evident in both the progressive red shift and increase in absorbance of the SPR with increasing local field associated with hotspots, observed in Figure 3. It should be noted, however, that in a study of the size dependence of nanostars by Khoury et al., the dependence of absorption strength and wavelength positioning of the SPR is not monotonic, and that with increasing reaction time, although the strength of the SPR continues to increase, the wavelength positioning ceases to redshift, and even begins to blue shift.

An interesting observation is made when the I_S/Nn signals of Figure 6c are normalised by the relative absorbance of each nanoparticle type, nanostar: nanotriangle: aggregated nanosphers, at the Raman excitation wavelength (15:10:1). As shown in Figure 6d, the normalised SERS signals overlap for all nanoparticle types, over the full range of concentrations of normalised dye concentrations. Therefore, despite the range of responses indicated for the different nanoparticle types and concentration ranges indicated in Figure 6a-c, the SERS responses can be mapped on to a single behaviour. Notably, the superlinear behaviour of Figure 6a has reduced to a slightly sublinear behaviour (slope = 0.93) for all nanoparticle types.

4. Discussion

The fundamental process of SERS is based on the local field enhancement in the region of metallic nanostructures upon excitation of the SPR [6, 32]. Gold nanoparticles and nanostructured substrates thus represent an ideal candidate for sensitive SERS detection and imaging in the visible region, as their SPR resonance occurs at 560nm [33]. However, increasingly, reports of optimised SERS

processes using gold nanoparticles and nanostructured substrates utilise longer source wavelengths of 633nm or 785nm [5, 34], indicating that it is not the intrinsic SPR of the gold nanoparticles which gives rise to the strong SERS effect.

The measurements presented here confirm that the SERS effect due to the SPR of isolated nanospheres (at 532nm) is negligible compared to that of nanosphere aggregates (at 785nm). In solution, as confirmed by DLS and TEM, the nanospheres spontaneously aggregate upon the addition of HCl, leading to a colour change from orange/red to blue-grey, as the SPR shifts from 560nm to ~660nm. Such junctions give rise to local field "hotspots" which are the source of the SERS effect in many studies, and are typically excited by source wavelengths of >600nm. For example, Drescher et al. have demonstrated that the acidic environment of endosomes causes nanoparticle aggregation into dimers and trimers leading to an increased SERS effect at 785 nm [16]. Bonifacio et al. have demonstrated that negligible SERS effects are observable in human serum samples, in which the serum proteins form a protein corona [33, 34], which coats the nanoparticles and prevents them from aggregating and forming hotspots, whereas, once the proteins are filtered out, strong and reproducible SERS signals can be recorded, again using 785 nm as source[35].

Thus, aggregation of nanoparticle provides hotspots which result in significantly higher SERS effects and the optimum source wavelength is considerably shifted from that of the SPR of the intrinsic nanoparticle. Braun et al. demonstrated that controlled aggregation can produce significant increases in the SERS response from silver nanoparticles[35]. Wustholtz et al. have explored structure-property relationships governing the SPR and SERS effects in gold nanosphere aggregates [36] and Laurence et al. have demonstrated good correlations of enhancement factors with degree of aggregation in encapsulated silver nanoaggregates [37]. The SERS response from substrates of hexagonally packed silver nanodiscs and nanorods has been demonstrated to vary over four orders of magnitude, dependent on the spacing [6]. However, aggregation is not a well controlled phenomenon and adds further uncertainty and variability to an already complex system. An alternative way to increase the local electromagnetic field associated with the SPR is to increase the local curvature of nanomaterials. It has been shown that when two spherical nanoparticles are aggregated or close enough, the SPR band is split into two components: longitudinal (low frequency) and transverse (high frequency) [38]. In spherical particles, these two modes (quadrupole and dipole) are not distinguishable from one another [39]. In the case of nanotriangles, due to their anisotropic shape, four different plasmon resonances have been observed: in-plane dipole, quadrupole, out-of-plane dipole, and quadrupole[40]. Nanostars contain a higher number of sharp corners and edges, and they have their own unique character as more complex anisotropically shaped nanoparticles and the modes oscillate at markedly different frequencies in both Au and Ag materials[41, 42]. Roughly, these modes originate from the degree and direction of polarization of the electron cloud relative to the incident electric field [43, 44].

Early theoretical simulations indicated that the local electric field enhancement in metal nanostructures is strongly dependent on the shape of the metal protrusion, both through the effectiveness of the so-called "lighting rod mechanism" and through the shape dependence of the SPR frequency [45, 46]. The lightning rod effect can result in the largest electric field near the sharpest surface, e.g., at the sharp ends of nanoparticles [47]. Nanotriangles contain three sharp vertices or ''tips'' of ~60 degrees that contribute significantly to their optical and electronic properties, although in practice, mixtures with varying degrees of tip truncation and rounding can be found. Nanostars contain ~5 or more vertices of angles ~ 30 degrees resulting in considerably higher local field enhancement and consequently higher SERS, per nanoparticle.

Much effort has been devoted to establishing a correlation between SERS and the absorbance of nanomaterials. Talley el al found aggregated nanospheres and dimers have higher absorbances at 700 and 785 nm respectively giving rise to higher SERS efficiencies [48]. Wustholz, K. L. et al also reported that SERS efficiency for aggregated nanospheres is related to the positioning of the SPR between 600-900 nm [36]. Similar work has been published recently comparing SERS from arrays of gold nanodisc with varied diameter and interdisc spacing [26]. In this study, the absorbance spectra of Figure 3 give a clear indication of the relationship between the nanoparticle absorbances and the nanoparticle structures. Notably, however, Khoury et al. have demonstrated that for nanostars monitored under controlled growth conditions the redshifting of the SPR resonance with reaction time is not monotonic [21]. The empirical observation of Figure 6c, that, when normalised for the nanoparticle absorbance at the Raman source wavelength, the SERS per nanoparticle overlaps for each nanoparticle type, indicates that this simple experimental parameter can be used as a guide to optimising nanoparticle synthesis and experimental design.

Conclusions

The study clearly demonstrates that the SERS signal due to the excitation of the SPR of isolated nanospheres is negligible compared to that of their aggregates, which requires longer wavelength excitation, in this instance at 785nm. Aggregation gives rise to local field hotspots which significantly enhance the local field, and red shift the SPR. A similar result, without the requirement of aggregation, can be achieved by increasing the local curvature of the nanoparticle surface, as is the case for nanotriangles and nanostars. The SERS effect for the common organic dye R6G is observed to systematically increase in the sequence nanospheres < nanosphere aggregates < nanotriangles < nanostars, as a result of the increased number and strength of local field hotspots.

The results presented here compare the SERS efficiencies of gold nanoparticles of differing shapes, but equivalent dimensions. The SERS intensity is seen to be well correlated with the optical absorption and indeed, when normalised to the absorbance at the Raman sources wavelength, the SERS intensity per nanoparticle, is seen to be equivalent for all nanoparticle types, indicating that optimisation of the SERS response can be achieved by optimising the absorbance of the nanoparticle at the Raman source wavelength.

Acknowledgement

F.B, A.C, and H.J.B acknowledge the support of Science Foundation Ireland 11/PI/1108. F.T. is funded under a Marie Curie Intra European Fellowship, Grant Agreement n° PIEF-GA-2012-332462.

References

1. C. Bao, N. Beziere, P. del Pino, B. Pelaz, G. Estrada, F. Tian, V. Ntziachristos, J. M. de la Fuente and D. Cui, *Small*, 2013, **9**, 68-74.
2. J. B. Jackson and N. J. Halas, *Proc Natl Acad Sci U S A*, 2004, **101**, 17930-17935.

3. S. Bhaskar, F. Tian, T. Stoeger, W. Kreyling, J. M. de la Fuente, V. Grazu, P. Borm, G. Estrada, V. Ntziachristos and D. Razansky, *Part Fibre Toxicol*, 2010, **7**, 3.
4. Bin Ren, Gennaro Picardi and B. Pettinger, *Review of Scientific Instruments*, 2004, **75**, 837-841.
5. J. L. J. PérezI, J. F. S. RamírezI, R. G. FuentesI, A. Cruz-OreaII and J. L. H. Pérez, *Brazilian Journal of Physics*, 2006, **36**
6. M. Moskovits, *hys Chem Chem Phys* 2013, **15**, 5301-5311.
7. P. K. Aravind and H. Metiu, *Surf Sci* 1983, **124**, 506–528.
8. K. Kneipp, H. Kneipp, I. Itzkan, R. R. Dasari and M. S. Feld, *J. Phys.: Condens. Matter* 2002, **14**, R597–R624.
9. P. K. Aravind and H. Metiu, *Chemical Physics Letters* 1980, **74**, 301–305.
10. P. K. Aravind, A. Nitzan and H. Metiu, *Surf Sci* 1981, **110**, 189–204.
11. Y. Fang, N. H. Seong and D. D. Dlott, *Science* 2008, **321**, 388–391.
12. V. S. Tiwari, T. Oleg, G. K. Darbha, W. Hardy, J. P. Singh and Paresh Chandra Ray, *Chemical Physics Letters*, 2007, **446**, 77-82.
13. F. Hao, C. L. Nehl, J. H. Hafner and P. Nordlander, *Nano Lett*, 2007, **7**, 729-732.
14. C. L. Nehl, H. Liao and J. H. Hafner, *Nano Lett*, 2006, **6**, 683-688.
15. C. Ziegler and A. Eychmüller, *J. Phys. Chem. C.* , 2011, **115**, 4502-4506.
16. D. Drescher, P. Guttmann, T. Buchner, S. Werner, G. Laube, A. Hornemann, B. Tarek, G. Schneider and J. Kneipp, *Nanoscale*, 2013, **5**, 9193-9198.
17. D. A. H. Hanaor, M. Michelazzi, C. Leonelli and C. C. Sorrell, *Journal of the European Ceramic Society*, 2012, **32**, 235–244.
18. D. Aherne, D. E. Charles, M. E. Brennan-Fournet, J. M. Kelly and Y. K. Gun'ko, *Langmuir*, 2009, **25**, 10165-10173.
19. B. Pelaz, V. Grazu, A. Ibarra, C. Magen, P. del Pino and J. M. de la Fuente, *Langmuir*, 2012, **28**, 8965-8970.
20. E. N. Esenturk and A. R. HightWalker, *J. Raman Spectrosc.* , 2009, **40**, 86–91.
21. C. G. Khoury and T. Vo-Dinh, *The journal of physical chemistryC, Nanomaterials and interfaces* 2008, **112**, 18849–18859.
22. S. M. Ali, F. Bonnier, A. Tfayli, H. Lambkin, K. Flynn, V. McDonagh, C. Healy, T. Clive Lee, F. M. Lyng and H. J. Byrne, *J Biomed Opt*, 2013, **18**, 061202.
23. J. Vura-Weis, M. D. Newton, M. R. Wasielewski and J. E. Subotnik, *J. Phys. Chem. C* 2010, **114**, 20449–20460.
24. A. Kudelski, *Chemical Physics Letters* 2005, **414**, 271-275.
25. R. Narayanan, R. J. Lipert and M. D. Porter, *Anal. Chem.*, , 2008, **80** 2265–2271.
26. Q. Yu, P. Guan, D. Qin, G. Golden and P. M. Wallace, *Nano Lett*, 2008, **8**, 1923-1928.
27. Félidj N, Aubard J, Lévi G, Krenn JR, Salerno M, Schider G, Lamprecht B, Leitner A and A. FR, *Phys Rev B* 2002, **65**, 075419.
28. J. E. Millstone, S. J. Hurst, G. S. Metraux, J. I. Cutler and C. A. Mirkin, *Small*, 2009, **5**, 646-664.
29. R. Jin, Y. Cao, C. A. Mirkin, K. L. Kelly, G. C. Schatz and J. G. Zheng, *Science*, 2001, **294**, 1901-1903.
30. G. Plascencia-Villa, D. Bahena, A. R. Rodriguez, A. Ponce and M. Jose-Yacaman, *Metallomics*, 2013, **5**, 242-250.
31. X. N. He, Y. Gao, M. Mahjouri-Samani, P. N. Black, J. Allen, M. Mitchell, W. Xiong, Y. S. Zhou, L. Jiang and Y. F. Lu, *Nanotechnology* 2012, **23**, 205702
32. D. Zhang, S. M. Ansar, K. Vangala and D. Jiang, *Journal of Raman Spectroscopy 41 :952–957.*, 2010, **41**, 952–957.
33. J. S. Gebauer, M. Malissek, S. Simon, S. K. Knauer, M. Maskos, R. H. Stauber, W. Peukert and L. Treuel, *Langmuir*, 2012, **28**, 9673-9679.
34. A. Bonifacio, S. Dalla Marta, R. Spizzo, S. Cervo, A. Steffan, A. Colombatti and V. Sergo, *Anal Bioanal Chem*, 2014, **406**, 2355-2365.
35. G. Braun, S. Lee, T. Laurence, N. Fera, L. Fabris, G. C. Bazan, M. Moskovits and N. O. Reich, *J Phys Chem C*, 2009, **113**, 13622–13629.
36. K. L. Wustholz, A. I. Henry, J. M. McMahon, R. G. Freeman, N. Valley, M. E. Piotti, M. J. Natan, G. C. Schatz and R. P. Van Duyne, *J Am Chem Soc*, 2010, **132**, 10903-10910.
37. T. A. Laurence, G. B. Braun, N. O. Reich and M. Moskovits, *Nano Lett.*, 2012, **12**, 2912–2917.
38. L. J. Sherry, R. Jin, C. A. Mirkin, G. C. Schatz and R. P. Van Duyne, *Nano Lett*, 2006, **6**, 2060-2065.
39. P. Mulvaney, *Langmuir*, , 1996, **12** 788–800.
40. S. L. Kleinman, R. R. Frontiera, A. I. Henry, J. A. Dieringer and R. P. Van Duyne, *Phys Chem Chem Phys* 2013, **15**, 21-36.
41. J. H. Seo, H. S. Park, Y. Yoo, T. Y. Seong, J. Li, J. P. Ahn, B. Kim and I. S. Choi, *Nano Lett*, 2013, **13**, 5112-5116.
42. P. S. Kumar, I. Pastoriza-Santos, B. Rodriguez-Gonzalez, F. J. G. de Abajo and L. M. Liz-Marzan, *Nanotechnology* 2008, **19**, 015606.
43. J. Rodríguez-Fernández, I. Pastoriza-Santon, J. Pérez-Juste, F. J. G. d. Abajo and a. L. M. Liz-Marzán, *J. Phys. Chem. C*, 2007, **111**, 13361–13366.
44. A. Wei, B. Kim, B. Sadtler and S. L. Tripp, *ChemPhysChem*, 2001, **2**, 743-745.
45. J. Gersten and A. Nitzan, *J Chem Phys* 1980, **73**, 3023–3037.
46. X. Zhang, C. R. Yonzon, M. A. Young, D. A. Stuart and R. P. Van Duyne, *IEE Proc., Nanobiotechnol.* , 2005, **152**, 195.
47. J. Hu, Z. Wang and J. Li, *Sensors (Basel)*, 2007, **7**, 3299–3311.
48. C. E. Talley, J. B. Jackson, C. Oubre, N. K. Grady, C. W. Hollars, S. M. Lane, T. Huser, P. Nordlander and N. J. Halas, *Nano Lett*, 2005, **5**, 1569-1574.